Hindawi
Journal of Nanomaterials
Volume 2020, Article ID 6196520, 7 pages
https://doi.org/10.1155/2020/6196520

Research Article

Facile-Controlled Epitaxial Growth Direction of Heterogeneous Core/Shell Structured $NaLnF_4$ Nanocrystals through Traditional Methods

Bing Xu,[1,2] Huimin Yang,[1] Xinru Lin,[1] and Dongyu Li[1,2]

[1]*Key Laboratory of Clean Energy Materials Chemistry of Guangdong Higher Education Institutes, Lingnan Normal University, Zhanjiang 524048, China*
[2]*Key Laboratory of Environmentally Friendly Functional Materials and Devices, Lingnan Normal University, Zhanjiang 524048, China*

Correspondence should be addressed to Dongyu Li; nanorainbows@163.com

Received 6 June 2020; Accepted 23 July 2020; Published 28 August 2020

Guest Editor: Peng Zhang

Fabrication of nanoscale materials with desirable morphology and surface properties becomes more urgent when constructing hybrid nanocrystals with multiple functionalities. Here, we report a facile measure to control the outer layer growth direction combining with coprecipitation and thermal decomposition method for constructing a series of heterogeneous core/shell structured $NaLnF_4$ nanocrystals, involving $NaYF_4$ and $NaNdF_4$ material. Our investigations suggest that it is feasible to control over the outer layer growth orientation by combining the two traditional methods.

1. Introduction

Purposeful design and fabrication of materials with desirable size, shape, and properties in nanoscale are attracting growing interest due to their own multifunctional performance [1–4]. Rare-earth-doped nanocrystals have recently emerged as a new generation of functional nanomaterials because they possess excellent optical and chemical properties. In particular, sodium rare-earth fluoride ($NaLnF_4$) nanocrystals, such as β-$NaYF_4$ [5–9], β-$NaGdF_4$ [10–13], β-$NaLuF_4$ [14, 15], β-$NaYbF_4$ [16, 17], or β-$NaNdF_4$, are widely used in biomedical field, security encoding, displays, photovoltaics, and so on. However, β-$NaLnF_4$ nanocrystals have a number of problems which limit their practical applications, including low emission efficiency associated with surface quenching effects, limited excitation light absorption coefficient, and limited functionalities for imaging and therapy. Constructing epitaxial core/shell-structured $NaLnF_4$ nanocrystals could address the challenges through effective passivation lattice defects on the surface of core particles, spatial confinement of different lanthanide dopants in separated shell layers to manipulate the energy transfer process, and introducing new functional layers into a single nanocrystal [2, 18–22].

There are three main approaches to produce high-quality $NaLnF_4$ and $NaLnF_4$-based core/shell-structured nanocrystals including hydrothermal, coprecipitation, and thermal decomposition methods [23–25]. Liu's group have achieved the precise size and shape control with atomic scale in a family of rare-earth-doped nanomaterials in the presence of various at oleate anions (OA^-)/(oleic acid molecules) OAH ratios by coprecipitation method [26]. Subsequently, they developed a hydrothermal-based epitaxial growth technique and found that EDTA or citric acid play an indispensable role in controlling epitaxial orientation [27]. Similar phenomena were observed by Zhang's group, they tuned the phase and morphology of the products by adjusting the composition of the oleic acid/NaOH ratio precisely in hydrothermal approach [25]. Zhao's group developed a thermal decomposition method to synthesize $NaLnF_4$ core-multishell-structured nanomaterials using the thermal decomposition method, and

the nanoparticles have a disk shape, indicating the $NaLnF_4$ shell growing in the [10$\bar{1}$0] direction [28]. But they did not explain the reason for this appearance further. High-quality homogeneous and heterogeneous core/shell structured nanoparticles could be constructed through the above methods and the morphology regulation of nanoparticles requires precise control of the proportion of reactants in the reaction solution.

Combined with the different methods of controlling the direction of shell growth in the above work, we used the β-$NaYF_4$ nanoparticles as core and coated the $NaNdF_4$ shell to construct monodisperse heterogeneous core/shell-structured $NaYF_4$/$NaNdF_4$ nanocrystals by the coprecipitation and thermal decomposition methods, respectively. This method is based on a selective epitaxial core/shell growth process in the presence of oleic acid molecular (OAH) or oleate anions (OA^-), which arises from the different sodium sources adopted in the two methods. OAH is often used as a coordination solvent during the synthesis of nanoparticles. Sodium hydroxide (NaOH), as sodium source in coprecipitation method, would cause OAH to dissociate into OA^-. Sodium trifluoroacetate (NaTFA), as a commonly used sodium source in thermal decomposition method, has no such effect on OAH. This allows us to introduce an approach to controlling the epitaxial growth direction of $NaLnF_4$ shell to construct heterogeneous core/shell-structured $NaLnF_4$ nanocrystals combining these two methods.

2. Experimental

2.1. Materials. $YCl_3{\cdot}6H_2O$ (99.9%), $NdCl_3{\cdot}6H_2O$ (99.9%), Nd_2O_3 (99.9%), oleic acid (90%) (OA), 1-octadecene (90%) (1-ODE), and trifluoroacetic acid (TFA) were all purchased from Sigma-Aldrich. NaOH (96.0%), NH_4F (96.0%), ethanol (99.7%), methanol (99.5%), and cyclohexane (99.5%) were purchased from Sinopharm Chemical Reagent Co., Ltd. Neodymium trifluoroacetate ($Nd(TFA)_3$) and yttrium trifluoroacetate ($Y(TFA)_3$) was prepared following our previous work [29]. All other chemical reagents were of analytical grade and used directly without further purification. Deionized water was used in all experiments.

2.2. Synthesis of Dumbbell-Like $NaYF_4$/$NaNdF_4$ Nanoparticles through the Coprecipitation Method. The dumbbell-like nanoparticles were synthesized following the method reported by Liu et al. with slight modifications. We first prepared β-$NaYF_4$ nanoparticles with a size of 25 nm and then coated $NaNdF_4$ shell with coprecipitation method. In a typical experiment, for the β-$NaYF_4$ nanoparticle synthesis, $YCl_3{\cdot}6H_2O$ (0.5 mmol) was added into a mixture of oleic acid (3 mL) and 1-octadecene (7.5 mL) in a 50 mL three-necked flask at room temperature. Under a nitrogen atmosphere and stirring, the mixture was heated at 150°C for 0.5 h to form lanthanide–oleate complexes. Thereafter, the reaction solution was cooled down to room temperature followed by the addition of a 5 mL methanol solution containing NaOH (1.25 mmol) and NH_4F (2 mmol). Subsequently, the mixture was heated at 70°C for 0.5 h to evaporate the methanol under vigorous stirring. The temperature was then increased to 120°C. After being maintained for 10 min, the reaction mixture was heated to 300°C at a heating rate of 15°C min^{-1} under a nitrogen atmosphere and stirring. Upon completion of the reaction at 300°C after 1 h, the solution was cooled down to room temperature. The resulting nanocrystals were collected by centrifugation, washed with a mixture of cyclohexane and ethanol several times, and dispersed in cyclohexane (2 mL) for $NaNdF_4$ shell growth.

The $NaNdF_4$ shell precursor was prepared by adding $NdCl_3{\cdot}6H_2O$ (0.5 mmol) into an oleic acid (5 mL) and 1-octadecene (5 mL) mixture in a 50 mL three-necked flask followed by heating at 150°C for 30 min before cooling down to 50°C. Subsequently, as-prepared $NaYF_4$ nanoparticles (0.5 mmol) dispersed in 2 mL of cyclohexane were added under vigorous stirring, and a 10 mL methanol solution of NaOH (1.25 mmol) and NH_4F (2 mmol) was injected into the reaction flask after 5 min. The resulting mixture was stirred below 50°C for at least 60 min, heated to 300°C under a nitrogen atmosphere and kept for 1 h, and then cooled down to room temperature. The resulting nanoparticles were precipitated by adding a mixture of methanol and cyclohexane, collected by centrifugation, washed with ethanol several times, and redispersed in 5 mL of cyclohexane.

2.3. Synthesis of Pie-Shaped $NaYF_4$/$NaNdF_4$ Nanoparticles through the Thermal Decomposition Method. $NaYF_4$ nanoparticles (0.5 mmol) dispersed in 2 mL of cyclohexane, and $Nd(TFA)_3$ (0.5 mmol) was added into an oleic acid (5 mL) and 1-octadecene (5 mL) mixture in a 50 mL three-necked flask followed by heating at 80°C for 20 min to remove cyclohexane. Subsequently, the reaction mixture was heated to 300°C under a nitrogen atmosphere and kept for 30 min, and then cooled down to room temperature. The treating process of the product is the same as above.

2.4. Synthesis of Nanoscale Hexagonal Prismatic through the Coprecipitation Method. $YCl_3{\cdot}6H_2O$ (1 mmol) was added into an oleic acid (10 mL) and 1-octadecene (10 mL) mixture in a 100 mL three-necked flask followed by heating at 150°C for 30 min before cooling down to 50°C. Subsequently, as-prepared pie-shaped $NaYF_4$/$NaNdF_4$ nanoparticles (0.5 mmol) dispersed in 5 mL of cyclohexane were added under vigorous stirring, and a 20 mL methanol solution of NaOH (2.5 mmol) and NH_4F (4 mmol) was injected into the reaction flask after 5 min. The resulting mixture was stirred below 50°C for 30 min, heated to 300°C under a nitrogen atmosphere and kept for 1 h, and then cooled down to room temperature. The resulting nanoparticles were precipitated by adding a mixture of methanol and cyclohexane, collected by centrifugation, washed with ethanol several times, and redispersed in 10 mL of cyclohexane.

2.5. Synthesis of Dumbbell-Like Nanoparticles with Three Rings through the Thermal Decomposition Method. Dumbbell-like $NaYF_4$/$NaNdF_4$ nanoparticles (0.5 mmol) dispersed in 5 mL of cyclohexane, and $Y(TFA)_3$ (1 mmol) was added into an oleic acid (10 mL) and 1-octadecene (10 mL) mixture in a 50 mL three-necked flask followed by heating at 80°C for 20 min to remove cyclohexane. Subsequently, the reaction mixture was heated to 300°C under a nitrogen atmosphere and kept for 30 min, and then cooled down to room

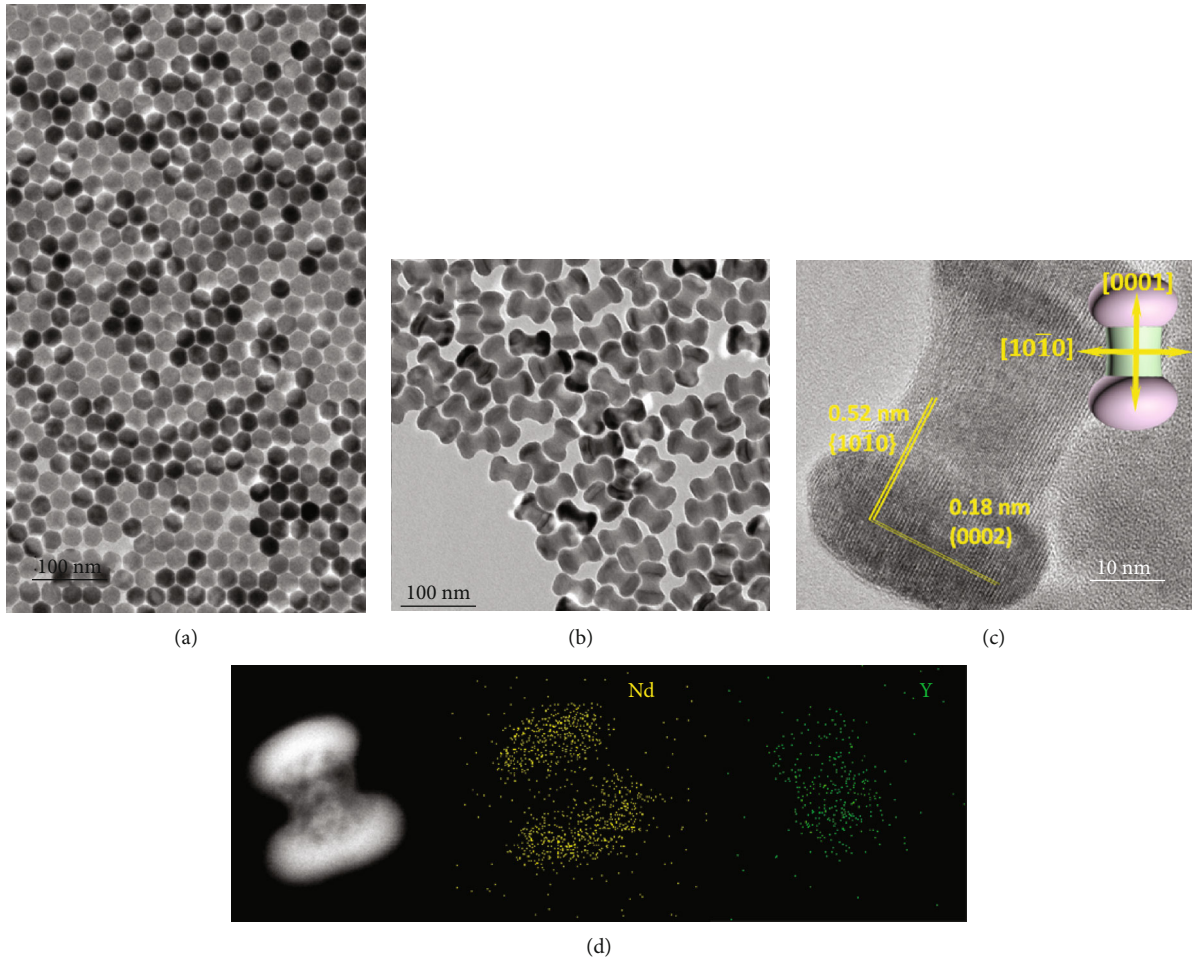

FIGURE 1: (a) TEM image of β-$NaYF_4$ nanoparticles, (b) TEM image, and (c) HRTEM image of dumbbell-like nanoparticles with epitaxial growth of $NaNdF_4$ shell in the [0001] direction (longitudinal growth). (d) Elemental mapping of the distribution of Nd^{3+} and Y^{3+} ions within a single dumbbell-like nanocrystal (inset in (c): schematic epitaxial growth of $NaNdF_4$ in the longitudinal direction).

temperature. The treating process of the product is the same as that of nanoscale hexagonal prismatic.

2.6. Characterization. Transmission electron microscopy (TEM) images were taken with a Tecnai G220 transmission electron microscope operating at 200 kV. High-resolution scanning transmission electron microscopy (STEM) and elemental mapping result were performed on a Tecnai G2 F30 transmission electron microscope operating at 300 kV. X-ray diffraction (XRD) patterns were recorded on a D/MAXRB X-ray diffractometer operated at 12 kW with Cu-Kα radiation ($\lambda = 1.5418$ Å).

3. Results and Discussion

We first prepared sub-25 nm β-$NaYF_4$ nanocrystals as seed particles (Figure 1(a)) and then coated $NaNdF_4$ shell on the β-$NaYF_4$ nanoparticles using the coprecipitation and thermal decomposition methods separately. Dumbbell-like $NaYF_4$/$NaNdF_4$ nanoparticles were obtained with a high uniformity (58 ± 3 nm in length, 35 ± 2 nm, and 18 ± 1 nm in diameter for each end and the middle bar) when the $NaNdF_4$ shell was coated by coprecipitation method (Figure 1(b)). HRTEM image depicted clearly lattice fringes associated with (10$\bar{1}$0) planes (d-spacing of 0.52 nm) and the (0002) plane (d-spacing of 0.18 nm) (Figure 1(c)), suggesting that the $NaNdF_4$ shell has grown in the [0001] direction (longitudinal growth). Elemental mapping of a single nanoparticle indicates that the Nd^{3+} ions are embedded at the dumbbell ends, and Y^{3+} ions are located in the middle of the dumbbell bars, respectively (Figure 1(d)). Furthermore, the middle diameter of the dumbbells is about 18 nm less than the diameter of $NaYF_4$ core, which showed that ligand etching had taken place on the side face ((10$\bar{1}$0) planes) of the $NaYF_4$ core during epitaxial growth.

We further demonstrated the formation of pie-shaped $NaYF_4$/$NaNdF_4$ nanocrystals by the thermal decomposition method (Figure 2(a)). It shows that the as-prepared nanoparticles were monodisperse with a diameter of 42 ± 2 nm. In view of the (10$\bar{1}$0) facets of β-$NaYF_4$ crystal with the same atomic arrangement, thus, the deposition rate of the $NaNdF_4$ shell on the (10$\bar{1}$0) facets of the β-$NaYF_4$ core must be the same. We believe that the ring-shaped $NaNdF_4$ shell growth in the [10$\bar{1}$0] direction (transverse growth). Considering the

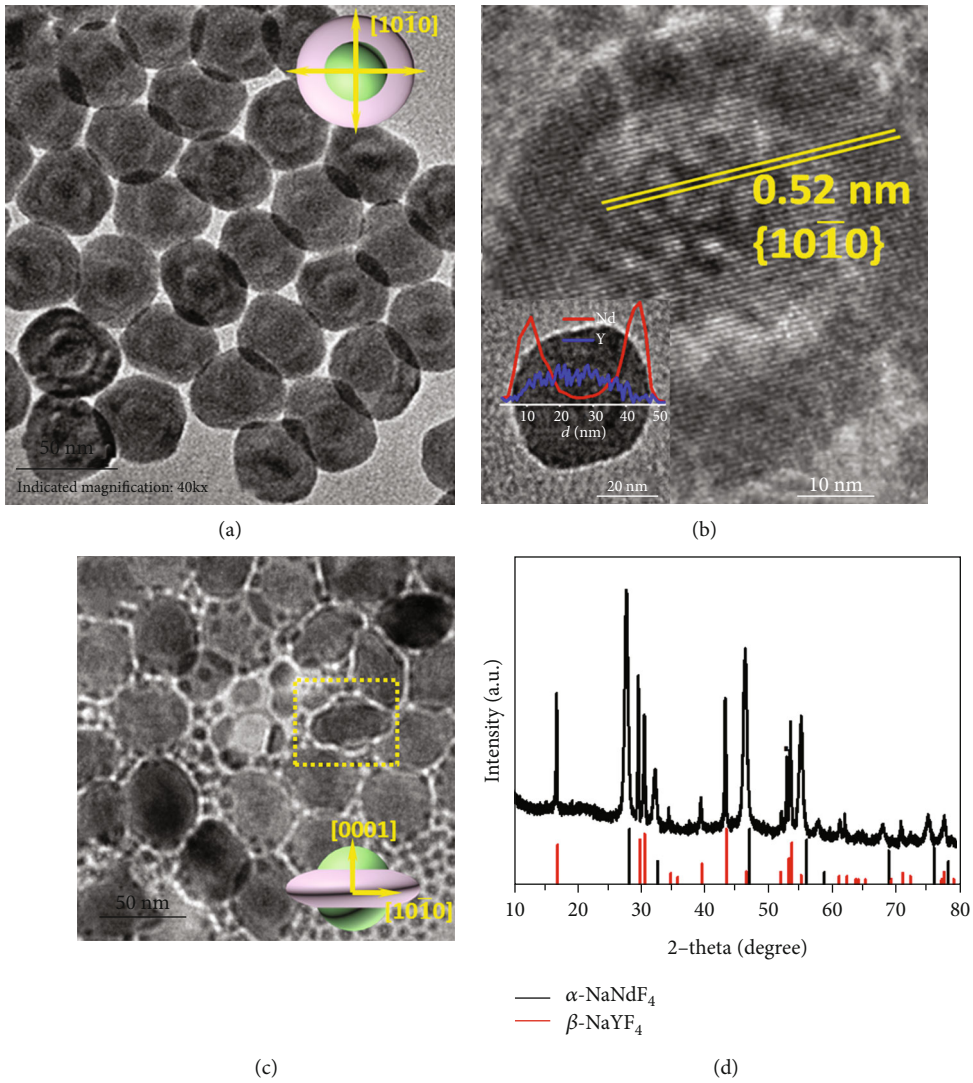

FIGURE 2: (a) TEM image and (b) HRTEM image of dumbbell-like nanoparticles with epitaxial growth of $NaNdF_4$ shell in the [10$\bar{1}$0] direction (transverse growth); (c) TEM image and (d) XRD patterns of nanoparticles obtained after 15 min of reaction (inset in (a) and (c): schematic epitaxial growth of $NaNdF_4$ in the transverse direction; inset in (b): elemental distribution of a single pie-shaped nanoparticle along the transverse direction).

diameter of $NaYF_4$ core is about 25 nm, the $NaNdF_4$ shell thickness is about 8.5 nm. The HRTEM image confirms that the nanoparticles were single-crystalline with an interplane distance of the lattice fringes of ~0.52 nm, which corresponds to that of the (0001) facets of β-$NaYF_4$ (Figure 2(b)). Lattice fringes associated with {10$\bar{1}$0} planes (d-spacing of 0.52 nm) can be discerned in the HRTEM image, and there are no obvious defect at the core-shell interface, suggesting that the $NaNdF_4$ shell has grown preferentially along the [0001] direction. Energy dispersive X-ray (EDX) line-scan profiles of a single pie-shaped nanoparticle confirms that the Nd^{3+} ions are embedded around the nanoparticle, and Y^{3+} ions are located in the center of it, respectively (inset in Figure 2(b)).

The TEM image of the products obtained after 15 min of reaction ($NaNdF_4$ shell coating time is 30 min) shows two distinct particle morphologies that include small nanospheres and large pie-like nanoparticles, well consistent with the presence of hexagonal and cubic phase $NaLnF_4$ observed by X-ray powder diffraction (Figure 2(d)). When the reaction time reached 30 minutes, the small cubic phase particles in the product disappeared. The result confirms that the shell precursor first formed cubic phase $NaNdF_4$ nanoparticles and then gradually coated on the β-$NaYF_4$ particles through the Oswald ripening process. The size along the [0001] direction, the part uncoated with outer layer, was almost unchanged (25 nm) (particle in dotted box in Figure 2(c)), indicating there is no obvious ligand etching phenomenon of $NaYF_4$ core when coating the $NaNdF_4$ shell through the thermal decomposition method.

To further confirm the influence of sodium sources on the shell growth direction, we coat the $NaYF_4$ shell on the as-prepared pie-shaped and dumbbell-like $NaYF_4$/$NaNdF_4$

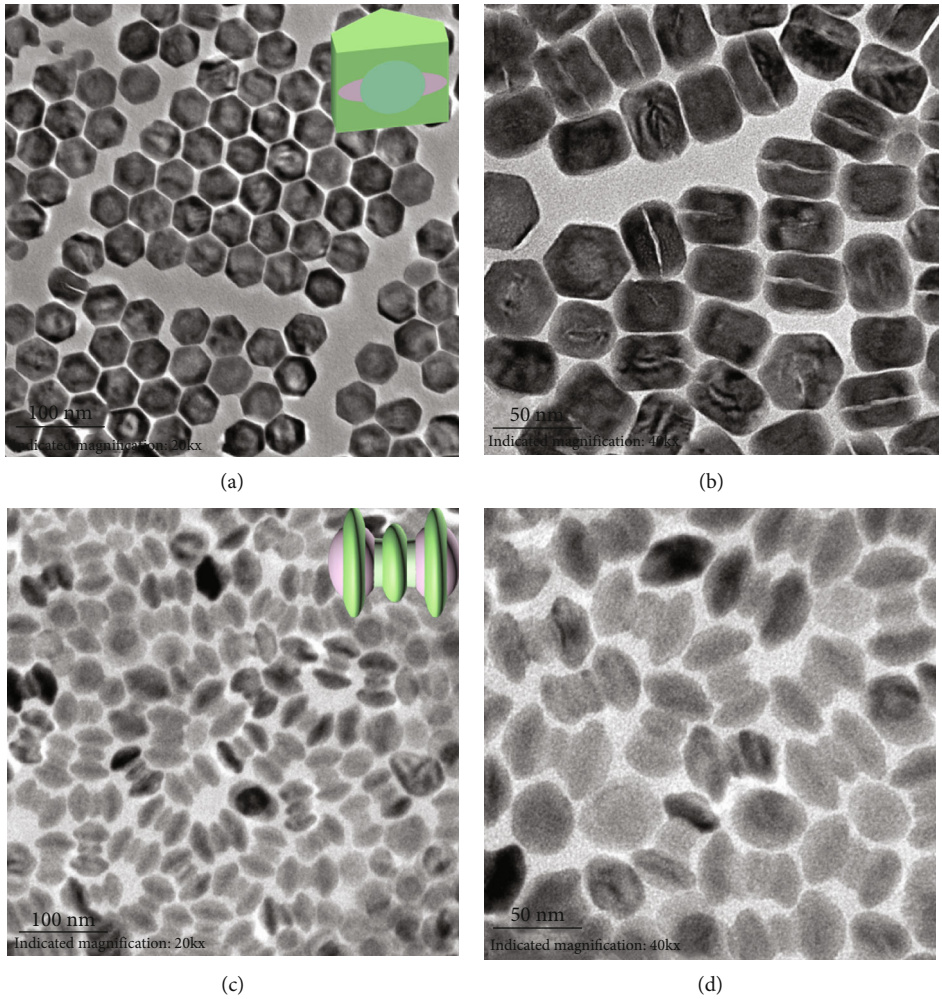

FIGURE 3: (a, b) TEM images of nanoscale hexagonal prismatic obtained from pie-shaped nanoparticles with $NaYF_4$ shell growing in the [0001] direction (longitudinal growth). (c, d) TEM images of nanoscale dumbbells with three rings around the side faces obtained from dumbbell-like nanoparticles with $NaYF_4$ shell growing in the $[10\bar{1}0]$ direction (transverse growth).

nanoparticles through the coprecipitation and thermal decomposition methods, respectively. Nanoscale hexagonal prismatic and dumbbells with three rings were obtained, respectively. As shown in Figures 3(a) and 3(b), the length of the hexagonal prismatic is about 38 nm, and the transverse size is about 43 nm, which indicated that the longitudinal growth is at least 13 nm and the transverse growth is only about 1 nm by contrast. A large number of hexagonal prisms have cracks in the side faces, which may be related to the lattice stress caused by the lattice mismatch between the $NaYF_4$ and $NaNdF_4$ crystals. When the $NaYF_4$ shell was coated on the dumbbells through thermal decomposition method, the transversal growth was observed, and the $NaYF_4$ rings were found around both ends and the middle of the dumbbell without a measurable change in the longitudinal direction (Figures 3(c) and 3(d)).

To reveal the underlying cause of these phenomena, we lay out the reaction parameters of the shell coating process: (i) For the coprecipitation and thermal decomposition method, the types and proportion of reaction solvents are identical (V/V(OA/1 – ODE) = 1/1). Types of rare-earth salts for shell precursors are different (rare earth chloride in coprecipitation method and rare earth trifluoroacetate salts in thermal decomposition method), but in the two-shell coating process, both shell precursors first form cubic phase $NaLnF_4$ nanoparticles and then wraps themselves on the inner layer when the shelling temperature exceed 270°C [22, 24, 30]. Therefore, we believe that the difference of precursor species is not the main reason for the different growth direction of shell; (ii) the sodium sources adopted in coprecipitation and thermal decomposition method are NaOH and NaTFA, respectively. As mentioned above, OH^- in the reaction solvent could dissociate OAH into OA^-, and OA^- preferentially binds to Y^{3+} ions exposed on the $(10\bar{1}0)$ facets of β-$NaYF_4$ nanocrystal, with a much higher binding energy (-35.4 eV) than that on the (0001) facet (-21.8 eV), which means that OA^- preferentially binds to Y^{3+} ions exposed on the $(10\bar{1}0)$ facet of the β-$NaYF_4$ nanocrystal [26]. Due to a large concentration of passivating OA^- ions on the $(10\bar{1}0)$ facets, a faster longitudinal deposition of $NaNdF_4$ shell on

the both (0001) facets of β-$NaYF_4$ core would occur compared with transversal deposition on the $(10\bar{1}0)$ facets. Meanwhile, the dissolution (etching) phenomenon from the side face of β-$NaYF_4$ core takes place, which was attributed to the strong binding of OA^- to the exposed Y^{3+} on the side surfaces in the presence of high concentration of OA^- [31]. As a result, dumbbell-like nanoparticles formed. In contrast, when NaTFA was adopted as sodium source in thermal decomposition method, NaTFA could not dissociate OAH to OA^-; thus, there are less OA^- in the reaction solution. Unlike OA^- ions, OAH binds to the (0001) facets with a higher probability (-9.4 eV) than the $(10\bar{1}0)$ facet (-4.6 eV), which means that the shell precursor would preferentially deposit on the $(10\bar{1}0)$ facet (side face). As a consequence, epitaxial growth of shell in the transversal direction was observed, and $NaNdF_4$ rings around the $NaYF_4$ core were formed. In addition, there were no obvious dissolution phenomenon takes places on the non-coated surface due to the weak binding of OAH to the exposed Y^{3+}. Based on these analyses, we suggest that sodium source in the preparation methods is playing a critical role on the epitaxial shell growth direction. (iii) The crystal lattice mismatch between inner layer and shell layer has influence on the epitaxial growth. Considering the morphology evolution of the core-shell-structured nanoparticles composed of β-$NaYF_4$ and β-$NaNdF_4$ involved in this work, the lattice mismatch between them may not be the main reason for the different direction of the epitaxial growth of the shell. Besides, this work does not explore the effect of temperature on the shell epitaxial growth. According to the previous work, the reaction temperature does not alter the direction of epitaxial growth but does affect the growth speed [26].

4. Conclusion

We have constructed heterogeneous core/shell-structured $NaLnF_4$ nanocrystals with various shapes using the traditional preparation methods. Microstructure results show that NaOH and NaTFA, as the sodium source, have different influence on the concentration ratio of OA- ions and OAH in the reaction solution and lead to longitudinal and transversal growth direction, respectively. We believe that the construction of heterostructure in nanoscale can be applied to precisely regulate the interparticle energy transfer. In addition, this work can be used to synthesize heterojunctions of other shell materials, such as $NaLuF_4$ and $NaGdF_4$. The addition of $NaLuF_4$ enables X-ray computed tomography, whereas using $NaGdF_4$ enables magnetic resonance imaging. Furthermore, these studies could be facilitated by harnessing the anisotropic properties of different types of layer that permit diverse functionalizations for multimodal applications.

Data Availability

Findings of this research work will be provided by the corresponding author on reasonable demand.

Conflicts of Interest

The authors declare no conflicts of interest.

Acknowledgments

This work was financially supported by the Natural Science Foundation of Guangdong Province (No. 2018A030307011, 2019A1515011228, and 2019A1515011461), Program of Young Creative Talents in Universities of Guangdong Province (No. 2018KQNCX153), Natural Science Foundation of Jiangxi Province (No. 20192ACBL21045), and National Natural Science Foundation of China (No. 61705095).

References

[1] J. Wang, R. Deng, M. A. MacDonald et al., "Enhancing multiphoton upconversion through energy clustering at sublattice level," *Nature Materials*, vol. 13, no. 2, pp. 157–162, 2014.

[2] R. Deng, F. Qin, R. Chen, W. Huang, M. Hong, and X. Liu, "Temporal full-colour tuning through non-steady-state upconversion," *Nature Nanotechnology*, vol. 10, no. 3, pp. 237–242, 2015.

[3] Y. W. Jun, J. S. Choi, and J. Cheon, "Shape control of semiconductor and metal oxide nanocrystals through nonhydrolytic colloidal routes," *Angewandte Chemie International Edition*, vol. 45, no. 21, pp. 3414–3439, 2006.

[4] B. Zhou, B. Shi, D. Jin, and X. Liu, "Controlling upconversion nanocrystals for emerging applications," *Nature Nanotechnology*, vol. 10, no. 11, pp. 924–936, 2015.

[5] L. Zeng, Y. Pan, Y. Tian et al., "Doxorubicin-loaded $NaYF_4$:Yb/Tm/TiO_2 inorganic photosensitizers for NIR-triggered photodynamic therapy and enhanced chemotherapy in drug-resistant breast cancers," *Biomaterials*, vol. 57, pp. 93–106, 2015.

[6] Z. Li, T. Liang, S. Lv, Q. Zhuang, and Z. Liu, "A rationally designed upconversion nanoprobe for in vivo detection of hydroxyl radical," *Journal of the American Chemical Society*, vol. 137, no. 34, pp. 11179–11185, 2015.

[7] Z. Li, S. Lv, Y. Wang, S. Chen, and Z. Liu, "Construction of LRET-based nanoprobe using upconversion nanoparticles with confined emitters and bared surface as luminophore," *Journal of the American Chemical Society*, vol. 137, no. 9, pp. 3421–3427, 2015.

[8] H. H. Gorris, R. Ali, S. M. Saleh, and O. S. Wolfbeis, "Tuning the dual emission of photon-upconverting nanoparticles for ratiometric multiplexed encoding," *Advanced Materials*, vol. 23, no. 14, pp. 1652–1655, 2011.

[9] N. M. Idris, M. K. Gnanasammandhan, J. Zhang, P. C. Ho, R. Mahendran, and Y. Zhang, "In vivo photodynamic therapy using upconversion nanoparticles as remote-controlled nanotransducers," *Nature Medicine*, vol. 18, no. 10, pp. 1580–1585, 2012.

[10] G. Chen, T. Y. Ohulchanskyy, S. Liu et al., "Core/shell $NaGdF_4$:Nd^{3+}/$NaGdF_4$ nanocrystals with efficient near-infrared to near-infrared downconversion photoluminescence for bioimaging applications," *ACS Nano*, vol. 6, no. 4, pp. 2969–2977, 2012.

[11] Y. Hou, R. Qiao, F. Fang et al., "$NaGdF_4$ nanoparticle-based molecular probes for magnetic resonance imaging of intraperitoneal tumor xenografts in vivo," *ACS Nano*, vol. 7, no. 1, pp. 330–338, 2012.

[12] C. Liu, Z. Gao, J. Zeng et al., "Magnetic/upconversion fluorescent $NaGdF_4$:Yb, Er nanoparticle-based dual-modal molecular

probes for imaging tiny tumors in vivo," *ACS Nano*, vol. 7, no. 8, pp. 7227–7240, 2013.

[13] N. J. J. Johnson, W. Oakden, G. J. Stanisz, R. Scott Prosser, and F. C. J. M. van Veggel, "Size-tunable, ultrasmall $NaGdF_4$ nanoparticles: insights into their T_1MRI contrast enhancement," *Chemistry of Materials*, vol. 23, no. 16, pp. 3714–3722, 2011.

[14] Q. Liu, Y. Sun, T. Yang, W. Feng, C. Li, and F. Li, "Sub-10 nm hexagonal lanthanide-doped $NaLuF_4$ upconversion nanocrystals for sensitive bioimaging in vivo," *Journal of the American Chemical Society*, vol. 133, no. 43, pp. 17122–17125, 2011.

[15] S. Zeng, J. Xiao, Q. Yang, and J. Hao, "Bi-functional $NaLuF_4$:Gd^{3+}/Yb^{3+}/Tm^{3+} nanocrystals: structure controlled synthesis, near-infrared upconversion emission and tunable magnetic properties," *Journal of Materials Chemistry*, vol. 22, no. 19, p. 9870, 2012.

[16] G. Chen, J. Shen, T. Y. Ohulchanskyy et al., "(alpha-$NaYbF_4$:Tm^{3+})/CaF_2 core/shell nanoparticles with efficient near-infrared to near-infrared upconversion for high-contrast deep tissue bioimaging," *ACS Nano*, vol. 6, no. 9, pp. 8280–8287, 2012.

[17] G. Tian, X. Zheng, X. Zhang et al., "TPGS-stabilized $NaYbF_4$:Er upconversion nanoparticles for dual-modal fluorescent/CT imaging and anticancer drug delivery to overcome multi-drug resistance," *Biomaterials*, vol. 40, pp. 107–116, 2015.

[18] G. Chen, T. Y. Ohulchanskyy, W. C. Law, H. Agren, and P. N. Prasad, "Monodisperse $NaYbF_4$:Tm^{3+}/$NaGdF_4$ core/shell nanocrystals with near-infrared to near-infrared upconversion photoluminescence and magnetic resonance properties," *Nanoscale*, vol. 3, no. 5, pp. 2003–2008, 2011.

[19] J. W. Shen, J. Wang, D. Kong, and X.-P. Yan, "Sub-20 nm sandwich-structured $NaGdF_4$:Yb/Tm @$NaLuF_4$:Yb/Tm@-$NaYF_4$ nanocrystals for in vivo upconversion luminescence/-computed tomography imaging," *RSC Advances*, vol. 4, no. 10, p. 5088, 2014.

[20] Y. Zhong, I. Rostami, Z. Wang, H. Dai, and Z. Hu, "Energy migration engineering of bright rare-earth upconversion nanoparticles for excitation by light-emitting diodes," *Advanced Materials*, vol. 27, no. 41, pp. 6418–6422, 2015.

[21] J. Song, O. Wang, H. Shen et al., "Over 30% external quantum efficiency light-emitting diodes by engineering quantum dot-assisted energy level match for hole transport layer," *Advanced Functional Materials*, vol. 29, no. 33, article 1808377, 2019.

[22] B. Xu, X. Zhang, W. Huang et al., "Nd^{3+} sensitized dumbbell-like upconversion nanoparticles for photodynamic therapy application," *Journal of Materials Chemistry B*, vol. 4, no. 16, pp. 2776–2784, 2016.

[23] F. Wang, R. Deng, and X. Liu, "Preparation of core-shell $NaGdF_4$ nanoparticles doped with luminescent lanthanide ions to be used as upconversion-based probes," *Nature Protocols*, vol. 9, no. 7, pp. 1634–1644, 2014.

[24] H. X. Mai, Y. W. Zhang, R. Si et al., "High-quality sodium rare-earth fluoride nanocrystals: controlled synthesis and optical properties," *Journal of the American Chemical Society*, vol. 128, no. 19, pp. 6426–6436, 2006.

[25] F. Zhang, Y. Wan, T. Yu et al., "Uniform nanostructured arrays of sodium rare-earth fluorides for highly efficient multicolor upconversion luminescence," *Angewandte Chemie International Edition*, vol. 46, no. 42, pp. 7976–7979, 2007.

[26] D. Liu, X. Xu, Y. Du et al., "Three-dimensional controlled growth of monodisperse sub-50 nm heterogeneous nanocrystals," *Nature Communications*, vol. 7, no. 1, article 10254, 2016.

[27] Y. Zhang, L. Huang, and X. Liu, "Unraveling epitaxial habits in the $NaLnF_4$ system for color multiplexing at the single-particle level," *Angewandte Chemie International Edition*, vol. 55, no. 19, pp. 5718–5722, 2016.

[28] X. Li, Z. Guo, T. Zhao et al., "Filtration shell mediated power density independent orthogonal excitations-emissions upconversion luminescence," *Angewandte Chemie International Edition*, vol. 128, no. 7, pp. 2510–2515, 2016.

[29] B. Xu, D. Li, Z. Huang, C. Tang, W. Mo, and Y. Ma, "Alleviating luminescence concentration quenching in lanthanide doped CaF2based nanoparticles through Na+ion doping," *Dalton Transactions*, vol. 47, no. 22, pp. 7534–7540, 2018.

[30] H.-X. Mai, Y.-W. Zhang, L.-D. Sun, and C.-H. Yan, "Size- and phase-controlled synthesis of monodisperse $NaYF_4$:Yb, Er nanocrystals from a unique delayed nucleation pathway monitored with upconversion spectroscopy," *Journal of Physical Chemistry C*, vol. 111, no. 37, pp. 13730–13739, 2007.

[31] C. Zhang and J. Y. Lee, "Prevalence of anisotropic shell growth in rare earth core-shell upconversion nanocrystals," *ACS Nano*, vol. 7, no. 5, pp. 4393–4402, 2013.